https://doi.org/10.5194/amt-2021-403
Preprint. Discussion started: 15 December 2021
© Author(s) 2021. CC BY 4.0 License.

Atmospheric Measurement Techniques Discussions

Look−up tables resolved by complex refractive index to correct particle sizes measured by common research−grade optical particle counters

Paola Formenti[1], Claudia Di Biagio[1], Yue Huang[2], Jasper Kok[2], Marc Daniel Mallet[1,*], Damien Boulanger[3], and Mathieu Cazaunau[1]

[1] Université de Paris and Univ Paris Est Creteil, CNRS, LISA, F−75013 Paris, France

[2] Department of Atmospheric and Oceanic Sciences, University of California Los Angeles, Los Angeles, CA 90095, USA

[3] Observatoire Midi-Pyrénées, CNRS, 31400 Toulouse, France

* now at: Institute for Marine and Antarctic Studies, University of Tasmania, Hobart, Tasmania, Australia.

Corresponding author: Paola Formenti (paola.formenti@lisa.ipsl.fr)

Abstract

Optical particle counters (OPCs) are widely used to measure aerosol particle number size distribution at atmospheric ambient conditions and over a large size range. Their measurement principle is based on the dependence of light scattering on particle size. However, this dependence is complex since it is not a monotonic function of size and because light scattering depends on the particle composition (i.e., the complex refractive index, *CRI*) and morphology. Therefore, the conversion of the measured scattered intensity to the desired particle size depends on the microphysical properties of the sampled aerosol population and whose relationship is not necessarily unique at all sizes. While these complexities have been addressed before, corrections are typically applied as needed and are not standardised. This issue is addressed here by providing a consistent database of precomputed correction factors for a wide range of complex refractive index values representing the variability in the

https://doi.org/10.5194/amt-2021-403
Preprint. Discussion started: 15 December 2021
© Author(s) 2021. CC BY 4.0 License.

composition of atmospheric aerosols. These correction factors are calculated for five different commercial OPCs (USHAS, PCASP, FSSP, GRIMM and its airborne version Sky−GRIMM, CDP) by assuming Mie theory for homogeneous spherical particles, and for the real part of the *CRI* between 1.33 and 1.75 in steps of 0.01 and the imaginary part between 0.0 and 0.4 in steps of 0.001. Correction factors for mineral dust are provided at a *CRI* of 1.53 – 0.003i and account for the asphericity of these particles. The datasets described in this paper are distributed through an open access repository: https://doi.org/10.25326/234 (license CC BY, Formenti et al., 2021) maintained by the French national center for Atmospheric data and services AERIS for data users and geophysicists who determine number size distribution measurements from OPCs in their atmospheric aerosol research. Application and caveats of the *CRI*-corrections factors are presented and discussed.

The dataset presented in this paper is not only useful for correcting the size distribution from OPCs when particle refractive indices are known, but also when this parameter can only be estimated. As well, this dataset can be used to calculate uncertainties or sensitivities associated with aerosol volume, mass, or extinction obtained from OPCs given little or no knowledge of the refractive index.

1. Introduction

Aerosol particles are some of the more elusive, but highly climate−relevant components of the atmosphere (Boucher et al., 2013). While airborne, aerosols interact with atmospheric radiation at wavelengths from the ultraviolet to the infrared, and serve as condensation nuclei for liquid and ice clouds (Seinfeld and Pandis, 2006). Upon deposition, they can change the productivity of marine and land ecosystems (Kanakidou et al., 2018). As well as directly influencing atmospheric composition by their emission, they also act as a sink for some reactive gases (e.g., Seinfeld and Pandis, 2006; Kanakidou et al., 2018). Through these processes aerosol particles affect the Earth's climate but they also can have adverse effects on the environment. In particular, aerosol particles can degrade air quality to the detriment of human health (Shiraiwa et al., 2017).

These varied effects of aerosols are largely due to by their broad size spectrum, which is. characterised by sizes ranging from a few nanometres to tens of micrometres depending on the sources and the mechanisms of emission, and on the transformations that they undergo whilst airborne (Seinfeld and Pandis, 2006). The typical particle size distribution in the atmosphere is a continuum of four lognormal modes (nucleation, comprising particles with diameters up to 10 nm; Aitken, comprising particles of diameters between 10 nm and 100 nm; accumulation, made up of particles with diameters from 100 nm to approximately 2.5 µm;

https://doi.org/10.5194/amt-2021-403
Preprint. Discussion started: 15 December 2021
© Author(s) 2021. CC BY 4.0 License.
Atmospheric Measurement Techniques Discussions

coarse, comprising particles with diameters larger than 2.5 μm), with different amplitudes, mode diameters, relative proportions, and chemical compositions (Seinfeld and Pandis, 2006). The nucleation, Aitken and most of the accumulation modes are due to condensation of precursors gases in the atmosphere, whereas particles in the coarse mode are mostly generated by wind friction on the sea and bare soil surfaces, and from biogenic or volcanic primary emissions. These modes are also characterised by different lifetimes in the atmosphere, ranging from a few minutes (nucleation mode) to days and weeks (Aitken, accumulation, and coarse modes).

Whilst the particle size distribution is a critical parameter to assess the effects of aerosols on radiation, clouds, chemistry, ocean and terrestrial productivity, and human health, its measurement is challenging. Instrumental techniques do not cover the entire particle size range, but only portions of it. Furthermore, these different instrumental techniques measure particle size using various operating principles, including light-scattering, aerodynamic and electric mobility properties of aerosol (Baron and Willeke, 2001; Hinds, 1999). Therefore, the particle size measured experimentally is an operational definition based on particle density, real and complex refractive index (*CRI*, the relation between spectral optical properties and chemical composition), and morphology (Baron and Willeke, 2001; Hinds, 1999).

Optical particle counters (OPCs) provide fast (better than 1 Hz) measurements over a large dynamic range, both in concentration and size, including sub− and super−micron particles (Baron and Willeke, 2001; Hinds, 1999; Wendisch and Brenguier, 2013). By adapting the geometry of the sensing volume and the wavelength of the light source, the design of the OPC can be customised to different applications (i.e., sampling mostly fine or coarse particles, more or less absorbing aerosols, minimise the effects of asphericity, etc.), therefore making them a versatile tool for atmospheric aerosol research. Research−grade OPCs are used worldwide in laboratory and field studies, including on research aircraft (Collins et al., 2000; Haywood et al., 2003a; 2003b; Reid et al., 2003; Osborne et al., 2008; Ryder et al., 2013; Di Biagio et al., 2015; Denjean et al., 2016; Petzold et al., 2009; Weinzerl et al., 2017; De Perim de Faria et al., 2017; Schafer et al., 2019; Brock et al., 2019; Wu et al., 2020).

The operating principle of the OPC is based on the fact that the intensity of monochromatic or white light scattered by an airborne particle (single or ensembles) in a given scattering direction depends on its size (Baron and Willeke, 2001; Hinds, 1999; Wendisch and Brenguier, 2013); and as a consequence, the intensity of light−scattering measured in a known sensing volume and at a known wavelength can be converted into particle size.

In principle, the scattering cross-section C_{sca} measured by an OPC can be converted into an optical equivalent diameter (D_{EO}) based on calibration with non−absorbing spherical particle

https://doi.org/10.5194/amt-2021-403
Preprint. Discussion started: 15 December 2021
© Author(s) 2021. CC BY 4.0 License.

Atmospheric Measurement Techniques Discussions

latex spheres (PSL) or equivalent scattering material of known *CRI* at the wavelength of light used in the instrument. However, this is complicated by the fact that atmospheric aerosols have different compositions (*CRI*) than the calibration material, and that the intensity of scattered light also depends on particle morphology (Dubovik et al., 2006; Huang et al., 2021). The differences in *CRI* and morphology between the calibration spheres and natural aerosols cause the OPC-determined size to be different from the real particle size. The error can propagate to size-relevant datasets, ultimately generating biases in the estimates of aerosol impacts on weather, climate, and human health (Huang et al., 2021). Henceforth, representing the number size distribution of the real atmospheric aerosol requires being able to convert the value of D_{EO} into an equivalent spherical particle geometrical (i.e., volume equivalent) diameter (D_{geo}) corresponding to the *CRI* of the sampled aerosols at the OPC operating wavelength.

In practice, the equivalence between D_{EO} at the reference *CRI* and D_{geo} at the *CRI* of the sampled aerosols is obtained by calculating, at each *CRI* value, the value of D_{geo} corresponding to the same scattering cross-section C_{sca} as that obtained when using D_{EO}. However, the scattering cross-section may not depend linearly or even monotonically on particle diameter. In the approximation of spherical particles, this effect is due to the Mie resonance and ripple oscillations in the light scattering functions. As a consequence, for a given *CRI* and D_{EO}, the scattering cross−section C_{sca} could correspond to a number of values of D_{EO}. This well−known and documented problem in the expert community (e.g., Garvey and Pinnick, 1983; Liu et al., 1992; Jaenicke and Hanusch, 1993; Pinnick et al., 2000; Collins et al., 2000; Reid et al., 2003; Osborne et al., 2008; Petzold et al., 2009; Rosenberg et al., 2012; Wendisch and Brenguier, 2013; Brock et al., 2016; 2019; Walser et al., 2017; Moore et al., 2021) and is illustrated in Figure 1 for C_{sca} characteristic functions of the CDP instrument (see Table 1). For selected *CRI* values corresponding to typical atmospheric aerosol types (see section 4), Figure 1 shows how a single value of C_{sca} can correspond to numerous particle diameters, with the exception of the case of highly-absorbing aerosols which causes the oscillations to be smoothed out. Additional uncertainties in the derived size distribution arise from the calibration of the instruments, as well as on their operation (counting statistics, flow rate, and sampling losses; e.g., Brock et al., 2019).

Various instrument and data users have reported solutions to these problems previously, corresponding to their interests and expertise:

1/ instrument developers and engineers have proposed processing methodologies taking into account the entire chain of instrument operations, in particular the size- and scattering-dependent calibrations (e.g., Rosenberg et al., 2012; Walser et al., 2017);

https://doi.org/10.5194/amt-2021-403
Preprint. Discussion started: 15 December 2021
© Author(s) 2021. CC BY 4.0 License.

2/ data users and geophysicists who rely on external expertise for calibration and instrument characterization and have proposed methods for adapting the measured size distribution to the ambient refractive indices, which have sometimes been evaluated using concurrent measurements of aerosol composition (e.g., Di Biagio et al. 2015; 2017; Denjean et al., 2016).

In this paper, we target the second category of scientists by providing standardized corrections for particle sizing calculations that account for the dependence of angular scattering on particle composition as represented by the *CRI*. Building on reported expert investigations, we address this technical note those who are regular or occasional users of data from some of the most common research−grade OPCs. Such data are available through open access datasets, which are becoming more and more popular through large−scale ground−based and airborne environmental research infrastructures, notably in several European organizations (e.g., Aerosol, Clouds and Trace Gases, ACTRIS, https://www.actris.fr/actris−eu/; In−service Aircraft for a Global Observing System, IAGOS, www.iagos.org; and EUropean Facility for Airborne Research, EUFAR https://www.eufar.net/) and within integrative science projects (e.g., the Global Aerosol Synthesis and Science Project, GASSP; Reddington et al., 2017). In using the data for their research and publications, these users are not necessarily data instrument operators, nor do they necessarily have the knowledge, expertise or time to perform and evaluate the *CRI*−adapted corrections.

This paper describes lookup tables of pre−computed scattering functions and size correction factors that are provided as downloadable ASCII files for a range of values of *CRI* relevant to atmospheric aerosols. Section 2 (Methods) presents the characteristics of the selected OPCs and the methodology used for the optical calculations and data presentation. Section 3 (Description of the datasets) presents the output files of the calculations that are available for interested users. Section 4 (Results) discusses the difficulties of the correction schemes and the associated caveats. Noted are the consequences of the lack of uniqueness in the relationship between particle diameter and scattering intensity and the influence of particle shape. Indeed, the calculations are performed under the assumption of spherical particles, which is a good approximation for a wide range of aerosol types and conditions. Additionally, a shape−dependent formulation is also applied to optimize the correction for aspherical mineral dust (e.g. Chou et al., 2008; Kandler et al., 2009; Huang et al., 2020), which is one of the most abundant aerosol types dominating the aerosol optical depth over large areas of the globe, in particular downwind of their source regions (Kok et al., 2021). Section 4 also presents the consequences on the representation of the size distribution and the calculation of optical properties for different methods commonly used to deal with sizes when the correction is not unique. Finally, section 5 provides the results and recommendations.

© Author(s) 2021. CC BY 4.0 License.

2. Methods

2.1. Instruments

Instruments considered in this paper are research−grade OPCs used for ambient atmospheric measurements and laboratory studies. Their nominal technical specifications are summarized in Table 1, which includes nominal size measurement range, light source wavelength, and range of scattering angles. The instruments are:

1. The Passive Cavity Aerosol Spectrometer Probe (PCASP, Model 100, Droplet Measurement Technologies, Boulder, CO) operates at 632.8 nm and measures light scattering between 35° and 145° collecting light from the direct and the reflected light beam (angular range 35°–120° and 60°–145°, respectively), so that light scattered between 60° and 120° will be counted twice. The particle number size distribution is determined over 31 channels for diameters between 0.1 and 3.0 μm (e.g., Liu et al., 1992; Reid and Hobbs, 1998; Rosenberg et al., 2012).
2. The Ultra High Sensitivity Aerosol Spectrometer (UHSAS, Droplet Measurement Technologies, Boulder, CO) has a ground−based version but the airborne version is most commonly used (e.g., Cai et al., 2008; Petzold et al., 2013; Brock et al., 2016; Kupc et al., 2018). It operates at 1054 nm and provides the number size distribution of particles with optical equivalent diameters ranging from 0.04 to 1 μm in 99 nominal size classes. The light scattering sensing angle range (22°−158°) reported by Cai et al. (2008) was subsequently corrected by Petzold et al. (2013) and Brock et al. (2016), who reported that the optically active range is circularly symmetric from 33° to 148°, with a blind region between 75.2 and 104.8°.
3. The Forward Scattering Spectrometer Probe (FSSP, Model 300, Droplet Measurement Technologies, Boulder, CO) is a widely used aircraft probe that measures light scattering at 632.8 nm in an optically active volume extending from 3 to 15° to retrieve the number size distribution in a nominal size range from 0.28 to 20.5 μm over 30 size classes (Baumgardner et al., 1992; Petzold et al., 2013).
4. The Cloud Droplet Probe (CDP, Model 300, Droplet Measurement Technologies, Boulder, CO) measures light scattering at 658 nm in an optically−active volume extending from 4° to 12° to retrieve the number size distribution in a nominal size range from 2 to 50 μm over 30 size classes (Baumgardner et al., 1992; Petzold et al., 2013).
5. The ground−based GRIMM and airborne Sky−OPC (Grimm Aerosol Technik, models 1.109 and 1.129, Ainring, Germany; hereafter the Sky−OPC will be named Sky−GRIMM) retrieve the particle number distribution over 31 size classes distributed for nominal diameters

https://doi.org/10.5194/amt-2021-403
Preprint. Discussion started: 15 December 2021
© Author(s) 2021. CC BY 4.0 License.

between 0.25 and 32 µm. These particle counters operate at 655 nm, and measure light scattered by the direct beam from 30° to 150° and by the reflected beam between 81° and 98° due to two face−to-face parabolic mirrors (opening angles of 120° and 18°, respectively) that collect light around a mean scattering angle of 90° (Heim et al., 2008). Like the PCASP, the light scattered between 81° and 98° has twice the weight relative to the intensity within 30°-81° and 98°-150°.

Table 1 also reports the reference material used for the calibration for each of the OPCs: NIST-certified polystyrene latex spheres (PSL) for the UHSAS, PCASP−100, FSSP−300, and GRIMM 1.109/Sky−OPC 1.129. The CDP is calibrated with non−absorbing glass bead reference particles. All these (spherical) reference materials have a refractive index of 1.59 – 0i at the light-source wavelength.

2.2. Optical calculations

Following Rosenberg et al. (2012), the scattering cross−section C_{sca} measured by an OPC is calculated as follows:

$$C_{sca} = \frac{\pi}{k^2} \int_0^{2\pi} \int_{\theta_{min}}^{\theta_{max}} \left(|\, S1(\theta, k\, D_p, CRI)\, |^2 + |\, S2(\theta, k\, D_p, CRI)\, |^2 \right) \sin(\theta)\, w_{optics}(\theta, \varphi)\, d\theta\, d\varphi \quad (1)$$

where

- k is the wavenumber of the light
- D_p is the particle diameter,
- *CRI* is the particle complex refractive index,
- *S1* is the light scattering intensity polarized in the parallel plane and *S2* in the perpendicular plane. Their squared absolute values, represented by bars in Equation 1, integrated over the scattering angle range characteristic of the OPCs is the total light intensity seen by the instrument;
- θ is the scattering angle between the incident laser beam and the viewing direction,
- φ is the azimuthal angle for a given scattering direction,
- $w_{optics}(\theta,\varphi)$ is a weighting function defined by the optical geometry of the OPC. As defined by Rosenberg et al. (2012), $w_{optics}(\theta,\varphi)$ takes into account the fact that, at certain angles, the PCASP and GRIMM/Sky−OPC measure scattered light both directly and after reflection by a mirror. In the case of rotational symmetry around the laser beam, $w_{optics}(\theta,\varphi)$ is a function of the scattering angle θ only.

https://doi.org/10.5194/amt-2021-403
Preprint. Discussion started: 15 December 2021
© Author(s) 2021. CC BY 4.0 License.
Atmospheric Measurement Techniques Discussions

Calculations are done according to two approximations:

- by assuming that particles are homogeneous spheres, the calculations use Mie theory according to Bohren and Huffman (2007). The particle diameter in Equation 1 is varied between 0.02 and 200 µm in logarithmically−equal steps of 0.004 (1001 values). The real part of the particle *CRI* (n) is varied between 1.33 and 1.75 (in steps of Δn = 0.01) and the imaginary part (k) from 0.0 to 0.4 (steps of Δk = 0.001) encompassing the range of values expected for atmospheric aerosols (e.g., Shettle and Fenn, 1992) at the working wavelengths of the OPCs;
- that the particles are ellipsoidal shaped to account for the asphericity of mineral dust particles according to Huang et al. (2021), who obtained single-scattering properties of ensembles of ellipsoidal dust particles by combining a shape-resolved single−particle scattering database (i.e., using the method of Meng et al. (2010) who combined four computational methods including Lorenz−Mie theory, T−matrix method, discrete dipole approximation, and an improved geometric optics method) with the globally representative shape distributions of dust aerosols (Huang et al., 2020). In this case, the *CRI* is set to 1.53 – 0.003i, at the upper limit of the values measured in the near-infrared for mineral dust aerosols (e.g., Fig. 8 in Di Biagio et al., 2019 which is a synthesis of the then current body of observations).

2.3. Calculation of equivalent particle diameter

Figure 1 shows that, due to non-monotonic behavior and oscillations, a given C_{sca} (from the nominal bin value) can be associated with several particle diameters (i.e., the value is not unique). The equivalence between D_{EO} at the reference *CRI* and D_{geo} at the aerosol *CRI* is obtained by calculating the C_{sca} from Mie theory for the wide range of particle sizes at the aerosol *CRI* and then, for each value of the bin size boundary (D_{bin}), using the particle size whose C_{sca} is closest to that calculated from D_{EO}, in both C_{sca} intensity and size. This equivalence is ultimately determined by the precision of the floating−point numbers (in our calculations they are 64−bit, double−precision).

For each size bin, the midpoint diameter D_{mid} is the geometric mean defined as follows:

$$D_{mid} = \sqrt{D_{bin,lower} * D_{bin,upper}} \quad (2)$$

where $D_{bin,lower}$ and $D_{bin,\,upper}$ are the lower and the upper bin diameter, respectively.

https://doi.org/10.5194/amt-2021-403
Preprint. Discussion started: 15 December 2021
© Author(s) 2021. CC BY 4.0 License.

The bin width (dlog*D*) is calculated as follows:

$$dlogD = log\left(\frac{D_{bin,upper}}{D_{bin,lower}}\right) \quad (3)$$

3. Description of the dataset

Three types of files in ASCII format are provided from this study:

1/ The values of scattering cross section C_{sca} for particle diameters between 0.02 and 200 µm in logarithmically equal steps of 0.004 and as a function of *CRI* (n=1.33−1.75; Δn=0.01, k=0.0-0.4; Δk=0.001) are provided in text files whose generic name is OPC_intensity_real_imag.txt, where *OPC* is the acronym of the particle counter, *real* is the value of the real part of the *CRI*, and *imag* is the imaginary part of the *CRI*. Each file contains four columns, namely

- the real part of the *CRI*
- the imaginary part of the *CRI*
- the particle diameter used in Equation 1 (in µm)
- the corresponding value of C_{sca} (in µm^2)

2/ the values of the corrected bin diameter as a function of *CRI* (n=1.33−1.75; Δn=0.01, k=0.0-0.4; Δk=0.001) are provided in text files whose generic name is OPC_Diameter_real_imag.out, where *OPC* is the acronym of the particle counter, *real* is the value of the real part of the *CRI*, and *imag* is the imaginary part of the *CRI*. Each file contains four columns, namely

- the nominal bin diameter (in µm) of the calibration *CRI*
- the bin diameter (in µm) calculated for the atmospheric *CRI*
- the bin midpoint diameter (D_{mid}, in µm) calculated for the atmospheric *CRI*
- the bin width (dlog*D*) calculated for the atmospheric *CRI*.

3/ The values of the corrected bin diameter in aspherical approximation for mineral dust are provided in text files whose generic name is OPC_Diameter_non_spherical_1.53000_0.00300000i, where OPC is the acronym of the particle counter. The format is equivalent to that of files OPC_Diameter_real_imag.out.

- the nominal bin diameter (in µm) of the calibration *CRI*
- the bin diameter (in µm) calculated for the atmospheric *CRI*
- the bin midpoint diameter (D_{mid}, in µm) calculated for the atmospheric *CRI*
- the bin width (dlog*D*) calculated for the atmospheric *CRI*.

https://doi.org/10.5194/amt-2021-403
Preprint. Discussion started: 15 December 2021
© Author(s) 2021. CC BY 4.0 License.

4. Example results

This section describes some of the elements of this analysis to help the reader understand the size correction factors available in the datasets. To do so, we use four example values of *CRI*, corresponding to non−absorbing material used for calibration (polystyrene latex spheres or equivalent light−scattering material; *CRI* = 1.59 – 0i), mineral dust (*CRI* = 1.53 – 0.003*i*; e.g., Fig. 8 in Di Biagio et al., 2019), urban aerosols (*CRI* = 1.56 – 0.087*i*; e.g., Radney and Zangmeister, 2018), and marine aerosols (*CRI* = 1.38 – 0.001*i*; e.g., Zieger et al., 2017).

4.1. Scattering function

The dependence of C_{sca} values on size for the example *CRI* values (**Figure 2**) allows exploration of a question: for a given value of *CRI*, is it possible to infer the particle size on the entire nominal size range of each OPC? The answer is not entirely affirmative. In general terms, the C_{sca} functions for wide−angle instruments (PCASP, UHSAS, and GRIMM/Sky−GRIMM,) are less affected by Mie oscillations than the forward−scattering instruments (FSSP−300 and CDP), and their behavior tends to be monotonic with size. However, the PCASP and the GRIMM/Sky−OPC curves tend to become more flat around 1 µm as the imaginary part of the *CRI* increases. In practical terms, this precludes the possibility of sizing absorbing particles in the range between 0.6 and 2 µm. For FSSP−300 and CDP, the determination of particle size is problematic in the range between 1 and 5 µm. On the contrary, for the UHSAS C_{sca} is monotonic in particle size for nearly the entire size range regardless of particle *CRI*, as discussed in Moore et al. (2021). As a metric of those considerations, **Figure 2** also shows the curves of the absolute values of dlogC_{sca}/dlog$D$ representing, for each value of the *CRI*, the rate of change of the scattering cross section across the size range. The value of dlogC_{sca}/dlog$D$ equal to 1 indicates that, for a given OPC, the dependence of the light-scattering cross section on particle size is linear, while the asymptotic value of 0 represents the situation when C_{sca} is independent of size and the OPC cannot be used to classify the particles. Oscillations and noisy behavior correspond to small scale oscillations, resulting in non-monotonic changes of C_{sca} with size. **Figure S1** extends this approach and shows, for each OPC considered in this paper, the contour plots of dlogC_{sca}/dlog$D$ as function of the bin midpoint diameters and the real and imaginary parts of *CRI*.

Figure 3 illustrates the effect of asphericity on the calculation of the scattering cross sections C_{sca} for moderately−absorbing mineral dust particles (*CRI* = 1.53 – 0.003*i*). As pointed out by Huang et al. (2021), calculating C_{sca} for homogeneous aspherical ellipsoid particles results in higher scattering for particles larger than approximately 1 µm. Because of the enhancement in particle surface area, accounting for dust asphericity in an ensemble of dust aerosols has the

https://doi.org/10.5194/amt-2021-403
Preprint. Discussion started: 15 December 2021
© Author(s) 2021. CC BY 4.0 License.

result of reducing the oscillations that affect the scattering functions in the spherical approximation.

4.2. Size correction factors

Figure 5 shows the scatterplot of the bin size boundary (D_{bin}) corresponding to the atmospheric *CRI* of the example aerosol types (mineral dust, urban and marine aerosols) compared to D_{bin} values obtained for the calibration *CRI*. The figure clearly illustrates the features that can appear, in particular for light absorption, which are evident around 1 µm and most prominent for OPCs that measure side scattering (i.e. PCASP and GRIMM/Sky-OPC). For UHSAS, the increase of the imaginary part of the *CRI* results in oscillations in the retrieved diameter in the upper part of the size domain, which depends strongly on the interpolation step used. For mineral dust, this is shown for both homogeneous spheres and aspherical ellipsoid particles. As expected from Figure 3, a more realistic representation of the shape distribution of mineral dust reduces the ambiguities of the OPC correction factors and significantly improves the resulting particle sizing. For a given D_{EO}, aspherical dust has a smaller D_{geo} than spherical dust for all the OPC models, because aspherical dust has a larger C_{sca} than volume-equivalent spherical dust (Fig. 2).

We therefore recommend care when using the values at sizes where the C_{sca} behavior is not monotonic. These instances can easily be identified by the values of dlog*D* provided in the OPC_Diameter_real_imag.out data files that are negative, corresponding to the corrected size of the upper bin (at atmospheric CRI) being smaller than the corrected size of the lower bin (Equation 3). As an illustration, Figures 5 and 6 help understand and evaluate the possible consequences on the representation of the number size distribution of mineral dust when the CDP is used in with corrections calculated using the spherical approximation. For the sake of generality, we use a model aerosol distribution reported by Seinfeld and Pandis (2006) that is expressed as the sum of three lognormal modes (see the Appendix for the formulae and modal parameters from the original Table 8.3 of the Seinfeld and Pandis (2006) publication). Figure 5 has three panels that show, for a *CRI* of 1.53−0.003*i*, the relationship between the corrected and the calibration bin diameters (left), the behavior of the corrected dlog*D* with calibration bin diameter (middle), and the representation of the size distribution using the corrected CDP evaluation of particle size (right). In the region between 4 and 10 µm, the increase of the calibration D_{bin} does not necessarily correspond to an increasing corrected D_{bin}, thereby resulting in a negative dlog*D* and in an evident discontinuity in the representation of the size distribution. In the literature, there are two families of data treatment methods that have been proposed to address this kind of occurrence:

https://doi.org/10.5194/amt-2021-403
Preprint. Discussion started: 15 December 2021
© Author(s) 2021. CC BY 4.0 License.
Atmospheric Measurement Techniques Discussions

1. grouping or widening of the bins of the OPCs (e.g., Johnson and Osborne, 2011), or excluding specific size ranges (e.g., Denjean et al., 2016) in order to eliminate instances of the scattering cross section flattening or decreasing with increasing size.
2. smoothing or fitting of the theoretical curves in order to eliminate oscillations (e.g., Liu et al., 1974; Hand and Kreidenweis, 2002; Covert et al., 1990; Johnson et al., 2008; Lance et al., 2010).

Figure 6 illustrates the application of these methods to a specific practical case, whose details described in Annex 1 of the supplementary material. For method 1, we grouped instances where dlog*D* was negative to create a wider bin and for which we assigned the sum of the particle counts of the original bins. For method 2, we fitted the D_{bin} curves with a second−degree polynomial function for each of the three size ranges reported in Annex 1 (a_0, a_1 and a_2 parameters in Table S2). Figure 6 shows that both methods improve the representation of the size distribution around 10 µm where the Mie oscillations are the most prominent. However, both choices have potential implications for the calculation of particle optical properties and mass concentrations. Table 2 shows an evaluation of these two methods by comparing the calculations of the optical properties of scattering, absorption and extinction using the two methods compared to those obtained with the base case in which the values of d*N*/*dlogD* corresponding to negative values of dlog*D* are simply discarded. Calculations are done at wavelengths relevant to modelling and remote sensing products (440, 550 and 870 nm, and 10 µm). It is clear that the data treatment influences their representation in a significant way, in particular by radically changing the spectral dependence of extinction and absorption at the shorter wavelengths (440 and 870 nm) (Table 3). Method 2 also results in increased scattering and extinction at 10 µm, due to the artificial increase of the particle number concentration at the highest diameters (not shown).

5. Summary and recommendations

In this paper, we describe a set of standardized corrections of particle sizing by OPC instruments in order to account for the dependence of angular scattering on particle composition, as represented by the particle complex refractive index *CRI*. This dataset of corrections is based on the simple assumption of homogeneous spherical particles and the use of Mie theory, and considers nominal OPC characteristics in terms of scattering angles of the sensing volume and wavelengths of the light sources. The approach covers the range of refractive indices expected for atmospheric aerosols, while, with the exception of mineral dust, it neglects the additional complexity due to the particle asphericity, which could be important for combustion aerosols.

https://doi.org/10.5194/amt-2021-403
Preprint. Discussion started: 15 December 2021
© Author(s) 2021. CC BY 4.0 License.
Atmospheric Measurement Techniques Discussions

In general terms, the analyses described confirm that research−grade OPC probes perform very well for the size ranges and for the particle types for which they were designed, as a result of careful design by experts in the field (see references in Table 1, and the overview of Wendisch and Brenguier (2003)). This contrasts with the relatively poor documentation of low-cost sensors that are indeed useful for complementary applications such as distributed monitoring of air quality (Hagan and Kroll, 2020). The behavior of light scattering intensity with size shown in Figure 2 indicates that the UHSAS performs very well for submicron particles with diameters less than 800 nm, regardless of their refractive index, and represents a very significant improvement compared to the PCASP instrument that operates on a similar, albeit more reduced size range. The FSSP, CDP, and GRIMM/Sky−OPC should be used to size particles larger than approximately 1 µm. However, GRIMM/Sky−GRIMM can be problematic in the range 1-2 µm. The FSSP and CDP can be problematic below 10 µm.

We recommend the users consider very carefully instances when light scattering is not monotonic with size, and use care when selecting the method for eliminating them. We recommend users to combine as much as possible, the retrieval of the particle size distribution from OPCs with concurrent, complementary measurements (e.g. particles sizers based on electrical mobility or aerodynamics, lidar measures of the backscattering vertical profile, gravimetric or composition measurements providing the mass concentration and composition) for optical and/or mass closure in order to ensure the robustness and consistency of the dataset, and improved knowledge of the *CRI*. Finally, and in order to make the best use of the possibilities offered by open data policies, we also recommend that users, whenever possible, to make contact with instrument operators to verify the specifics of the OPCs, their calibration, and their performance during field operations.

Finally, the significant sensitivity of the light scattering intensity C_{sca} to the particle *CRI* suggests the following considerations:

- diameters corrected for the *CRI* should be used rather than the calibration diameters even if particle *CRI* is not precisely known. Even with an approximate assumption of the particle origin (i.e. wind direction, time of day, season of year, air mass trajectory), assuming an aerosol type and/or *CRI* based on these other environmental conditions and using the corresponding *CRI*-corrected diameter is likely to be more accurate than using the calibration diameters;
- The dataset presented in this paper can also be used without any knowledge of the particle refractive index, or to deduce the refractive index of the aerosol if other instruments are available for closure or if more than one OPC are used. This approach can also provide uncertainty or sensitivity of size distribution estimates.

https://doi.org/10.5194/amt-2021-403
Preprint. Discussion started: 15 December 2021
© Author(s) 2021. CC BY 4.0 License.

Atmospheric Measurement Techniques Discussions

Acknowledgments

P. Formenti thanks Prof. A. Petzold (Forschungszentrum Jülich GmbH, Germany), Dr. C. Perez Garcia Pando (Barcelona Supercomputing Center, Spain) and Prof. J. F. Doussin (LISA, France) for useful discussions and encouragement. Prof. C. Cantrell is acknowledged for careful reading and improving of the manuscript.

Financial support

This work has received funding from the European Union's Horizon 2020 research and innovation programme through the EUROCHAMP–2020 Infrastructure. Activity was supported under grant agreement no. 730997 as well as from the project DustClim, part of ERA4CS, an ERA−NET initiated by JPI Climate, and funded by FORMAS (SE), DLR (DE), BMWFW (AT), IFD (DK), MINECO (ES), ANR (FR) with co−funding by the European Union (Grant 690462). funding by the European Union (Grant 690462). Y. Huang acknowledges the financial support from the National Aeronautics and Space Administration (NASA) grant 80NSSC19K1346, awarded under the Future Investigators in NASA Earth and Space Science and Technology (FINESST) program.

J. F. Kok acknowledges the support by the National Science Foundation (NSF) under grants 1552519 and 1856389 and the Army Research Office under Cooperative Agreement Number W911NF-20-2-0150. The views and conclusions contained in this manuscript are those of the authors and should not be interpreted as representing the official policies, either expressed or implied, of the Army Research Office or the US Government.

Data availability

The datasets described in this paper are distributed at open-access repository: https://doi.org/10.25326/234 (license CC BY, Formenti et al., 2021) maintained by the French national center for Atmospheric data and services, AERIS. Optical calculations with Mie theory for homogeneous spherical particles have been performed with the IDL mie_single.pro routine available at http://www.atm.ox.ac.uk/code/mie/mie_single.html).

Competing interests.

The authors declare no conflict of interest.

Special issue statement

This article is not part of a special issue. It is not associated with a conference.

Author contribution

https://doi.org/10.5194/amt-2021-403
Preprint. Discussion started: 15 December 2021
© Author(s) 2021. CC BY 4.0 License.

PF and CDB performed the calculations in the spherical mode and the full data analysis. YH and JFK performed the optical calculations in the aspherical mode. DB provided curation and distribution of the data. MDM and MC provided insight on data analysis and performed literature searches. PF wrote the manuscript with contributions from all co–authors.

References

Baron, P. A., and Willeke, K.: Aerosol measurement: Principles, techniques and applications, 2nd ed., John Wiley and Sons, New York, 2001.

Baumgardner, D., Dye, J. E., Gandrud, B. W., and Knollenberg, R. G.: Interpretation of measurements made by the forward scattering spectrometer probe (FSSP−300) during the Airborne Arctic Stratospheric Expedition, Journal of Geophysical Research: Atmospheres, 97, 8035−8046, https://doi.org/10.1029/91JD02728, 1992.

Baumgardner, D., Jonsson, H., Dawson, W., O'Connor, D., and Newton, R.: The cloud, aerosol and precipitation spectrometer: a new instrument for cloud investigations, Atmospheric Research, 59−60, 251−264, https://doi.org/10.1016/S0169−8095(01)00119−3, 2001.

Bohren, C. F., and Huffman, D. R.: Absorption and Scattering of Light by Small Particles, Wiley−VCH Verlag GmbH, 1983.

Boucher, O., Randall, D., Artaxo, P., Bretherton, C., Feingold, G., Forster, P., Kerminen, V.−M., Kon−do, Y., Liao, H., Lohmann, U., Rasch, P., Satheesh, S.K., Sherwood, S., Stevens B., and Zhang X. Y., Clouds and Aerosols. In: Climate Change 2013: The Physical Science Basis. Contribu−tion of Working Group I to the Fifth Assessment Report of the Intergovernmental Panel on Climate Change [Stocker, T.F., D. Qin, G.−K. Plattner, M. Tignor, S.K. Allen, J. Boschung, A. Nauels, Y. Xia, V. Bex and P.M. Midgley (eds.)]. Cambridge University Press, Cambridge, United Kingdom and New York, NY, USA, 2013.

Brock, C. A., Wagner, N. L., Anderson, B. E., Attwood, A. R., Beyersdorf, A., Campuzano−Jost, P., Carlton, A. G., Day, D. A., Diskin, G. S., Gordon, T. D., Jimenez, J. L., Lack, D. A., Liao, J., Markovic, M. Z., Middlebrook, A. M., Ng, N. L., Perring, A. E., Richardson, M. S., Schwarz, J. P., Washenfelder, R. A., Welti, A., Xu, L., Ziemba, L. D., and Murphy, D. M.: Aerosol optical properties in the southeastern United States in summer – Part 1: Hygroscopic growth, Atmos. Chem. Phys., 16, 4987–5007, https://doi.org/10.5194/acp−16−4987−2016, 2016.

Brock, C. A., Williamson, C., Kupc, A., Froyd, K. D., Erdesz, F., Wagner, N., Richardson, M., Schwarz, J. P., Gao, R.−S., Katich, J. M., Campuzano−Jost, P., Nault, B. A., Schroder, J. C., Jimenez, J. L., Weinzierl, B., Dollner, M., Bui, T., and Murphy, D. M.: Aerosol size distributions during the Atmospheric Tomography Mission (ATom): methods, uncertainties, and data products, Atmos. Meas. Tech., 12, 3081–3099, https://doi.org/10.5194/amt−12−3081−2019, 2019.

Cai, Y., Montague, D. C., Mooiweer−Bryan, W., and Deshler, T.: Performance characteristics of the ultra high sensitivity aerosol spectrometer for particles between 55 and 800 nm: Laboratory and field studies, J. Aerosol Sci., 39, 759–769, doi:10.1016/j.jaerosci.2008.04.007, 2008.

Collins, D. R., Johnsson, H. H., Seinfeld, J. H., Flagan, R. C., Gassó, S., Hegg, D. A., Russell, P. B., Schmid, B., Livingston, J. M., Öström, E., Noone, K. J., Russell, L. M., and Putaud, J. P.: In situ aerosol size distributions and clear column radiative closure during ACE−2, Tellus, 52B, 498 − 525, 2000.

Covert, D. S., Heintzenberg, J., and Hansson, H. C.: Electrooptical detection of external mixtures in aerosols, Aerosol Sci. Tech., 12, 446–456, 1990.

Crilley, L. R., Shaw, M., Pound, R., Kramer, L. J., Price, R., Young, S., Lewis, A. C. and Pope, F. D.: Evaluation of a low−cost optical particle counter (Alphasense OPC−N2) for 28ambient air monitoring, Atmospheric Measurement Techniques, 11(2), 709–720, 29doi:https://doi.org/10.5194/amt−11−709−2018, 2018.

https://doi.org/10.5194/amt-2021-403
Preprint. Discussion started: 15 December 2021
© Author(s) 2021. CC BY 4.0 License.

Atmospheric Measurement Techniques Discussions

Denjean, C., Cassola, F., Mazzino, A., Triquet, S., Chevaillier, S., Grand, N., Bourrianne, T., Momboisse, G., Sellegri, K., Schwarzenbock, A., Freney, E., Mallet, M., and Formenti, P.: Size distribution and optical properties of mineral dust aerosols transported in the western Mediterranean, Atmos. Chem. Phys., 16, 1081−1104, doi:10.5194/acp−16−1081−2016, 2016.

Di Biagio, C., L. Doppler, C. Gaimoz, N. Grand, G. Ancellet, J.−C. Raut, M. Beekmann, A. Borbon, K. Sartelet, J.−L. Attié, F. Ravetta, P. Formenti, Continental pollution in the Western Mediterranean basin: vertical profiles of aerosol and trace gases measured over the sea during TRAQA 2012 and SAFMED 2013, Atmos. Chem. Phys., 15, 9611−9630, doi:10.5194/acp−15−9611−2015, 2015

Di Biagio, C., Formenti, P., Balkanski, Y., Caponi, L., Cazaunau, M., Pangui, E., Journet, E., Nowak, S., Caquineau, S., Andreae, M. O., Kandler, K., Saeed, T., Piketh, S., Seibert, D., Williams, E., and Doussin, J.−F.: Global scale variability of the mineral dust long−wave refractive index: a new dataset of in situ measurements for climate modeling and remote sensing, Atmos. Chem. Phys., 17, 1901−1929, doi:10.5194/acp−17−1901−2017, 2017.

Di Biagio, C., Formenti, P., Balkanski, Y., Caponi, L., Cazaunau, M., Pangui, E., Journet, E., Nowak, S., Andreae, M. O., Kandler, K., Saeed, T., Piketh, S., Seibert, D., Williams, E., and Doussin, J.-F.: Complex refractive indices and single-scattering albedo of global dust aerosols in the shortwave spectrum and relationship to size and iron content, Atmos. Chem. Phys., 19, 15503–15531, https://doi.org/10.5194/acp-19-15503-2019, 2019.

Dubovik, O., A. Sinyuk, T. Lapyonok, B. N. Holben, M. Mishchenko, P. Yang, T. F. Eck, Volten, H., Muñoz, O., Veihelmann, B., W. J. van der Zande, Leon, J.−F., Sorokin, M., and Slutsker, I.: Application of spheroid models to account for aerosol particle nonsphericity in remote sensing of desert dust, J. Geophys. Res., 111, doi:10.1029/2005JD006619, 2006.

Flores, J. M., Trainic, M., Borrmann, S., and Rudich, Y.: Effective broadband refractive index retrieval by a white light optical particle counter, Physical Chemistry Chemical Physics, 11, 7943−7950, 2009.

Garvey, D. M., and R. G. Pinnick, Response Characteristics of the Particle Measuring Systems Active Scattering Aerosol Spectrometer Probe (ASASP–X), Aerosol Science and Technology, 2:4, 477−488, DOI: 10.1080/02786828308958651(1983).

Grimm, H., and Eatough, D. J.: Aerosol measurement: the use of optical light scattering for the determination of particulate size distribution, and particulate mass, including the semi−volatile fraction, J. Air Waste Manag. Assoc., 59, 101–107, doi:10.3155/1047−3289.59.1.101, 2009.

Formenti, P., C. Di Biagio, Y. Huang, J. Kok, M. D. Mallet, D. Boulanger, and M. Cazaunau, Look−up tables resolved by complex refractive index to correct particle sizes measured by common research−grade optical particle counters, https://doi.org/10.25326/234, 2021.

Hagan, D. H. and Kroll, J. H.: Assessing the accuracy of low-cost optical particle sensors using a physics-based approach, Atmos. Meas. Tech., 13, 6343–6355, https://doi.org/10.5194/amt-13-6343-2020, 2020.

Hand, J. L. and Kreidenweis, S. M.: A New Method for Retrieving Particle Refractive Index and Effective Density from Aerosol Size Distribution Data, Aerosol Sci. Tech., 36, 1012–1026, 2002.

Haywood, J. M., Osborne, S. R., Francis, P. N., Keil, A., Formenti, P., Andreae, M. O., and Kaye, P. H.: The mean physical and optical properties of regional haze dominated by biomass burning aerosol measured from the C−130 aircraft during SAFARI 2000, J. Geophys. Res., 108, 8473, 10.1029/2002jd002226, 2003a.

Haywood, J. M., Francis, P., Osborne, S., Glew, M., Loeb, N., Highwood, E., Tanré, D., Myhre, G., Formenti, P., and Hirst, E.: Radiative properties and direct radiative effect of Saharan dust measured by the C−130 aircraft during SHADE: 1. Solar spectrum, J. Geophys. Res., 108, doi:10.1029/2002JD002687, doi:10.1029/2002JD002687, 2003b.

Heim, M., Mullins, B. J., Umhauer, H., and Kasper, G.: Performance evaluation of three optical particle counters with an efficient "multimodal" calibration method, Journal of Aerosol Science, 39, 1019−1031, 2008.

Hinds, W. C.: Aerosol technology: properties, behavior, and measurement of airborne particles, John Wiley & Sons, Chichester, 504 pp., 1999.

Huang, Y., Kok, J. F., Kandler, K., Lindqvist, H., Nousiainen, T., Sakai, T., Adebiyi, A., and Jokinen, O.: Climate Models and Remote Sensing Retrievals Neglect Substantial Desert Dust Asphericity, Geophys. Res. Lett., 47, 475, e2019GL086592, 2020a, https://doi.org/10.1029/2019GL086592.

Huang, Y., Adebiyi, A. A., Formenti, P., & Kok, J. F. (2021). Linking the different diameter types of aspherical desert dust indicates that models underestimate coarse dust emission. Geophysical Research Letters, 48, e2020GL092054. https://doi.org/10.1029/2020GL092054

Kanakidou, M., Stelios Myriokefalitakis and Kostas Tsigaridis, Aerosols in atmospheric chemistry and biogeochemical cycles of nutrients, Environmental Research Letters, 13, 2018

Kandler, K. et al. (2009), Size distribution, mass concentration, chemical and mineralogical composition and derived optical parameters of the boundary layer aerosol at Tinfou, Morocco, during SAMUM 2006, Tellus, Ser. B Chem. Phys. Meteorol., 61(1), 32–50, doi:10.1111/j.1600-0889.2008.00385.x.

Kok, J. F., A. A. Adebiyi, S. Albani, Y. Balkanski, R. Checa-Garcia, M. Chin, P. R. Colarco, D. S. Hamilton, Y. Huang, A. Ito, M. Klose, D. M. Leung, L. Li, N. M. Mahowald, R. L. Miller, V. Obiso, C. Pérez García-Pando, A. Rocha-Lima, J. S. Wan, and C. A. Whicker (2021), Improved representation of the global dust cycle using observational constraints on dust properties and abundance, Atmospheric Chemistry and Physics, 21, 8127-67.

Kupc, A., Williamson, C., Wagner, N. L., Richardson, M., and Brock, C. A.: Modification, calibration, and performance of the Ultra-High Sensitivity Aerosol Spectrometer for particle size distribution and volatility measurements during the Atmospheric Tomography Mission (ATom) airborne campaign, Atmos. Meas. Tech., 11, 369–383, https://doi.org/10.5194/amt-11-369-2018, 2018.

Jaenicke, R. and Hanusch, T.: Simulation of the Optical Particle Counter Forward Scattering Spectrometer Probe 100 (FSSP−100), Aerosol Science and Technology, 18(4), 8309–322, doi:10.1080/02786829308959607, 1993

Johnson, B. T., S. R. Osborne, J. M. Haywood, and M. A. J. Harrison (2008), Aircraft measurements of biomass burning aerosol over West Africa during DABEX, J. Geophys. Res., 113, D00C06, doi:10.1029/2007JD009451

Johnson, B. T. and Osborne, S. R.: Physical and optical properties of mineral dust aerosol measured by aircraft during the GERBILS campaign, Q. J. Roy. Meteor. Soc., 137, 1117–1130, 2011.

Lance, S., Brock, C. A., Rogers, D., and Gordon, J. A.: Water droplet calibration of the Cloud Droplet Probe (CDP) and inflight performance in liquid, ice and mixed−phase clouds during ARCPAC, Atmos. Meas. Tech., 3, 1683–1706, doi:10.5194/amt−3−1683−2010, 2010.

Liu, B. Y. H., Berglund, R. N., and Agarwal, H. K.: Experimental studies of Optical Particle Counters, Atmos. Environ., 8, 717–732, 1974.

Liu, P. S. K., W. R. Leaitch, J. W. Strapp, and M. A. Wasey, Response of Particle Measuring Systems Airborne ASASP and PCASP to NaCl and Latex Particles, Aerosol Science and Technology, 16:2, 83−95, DOI: 10.1080/02786829208959539, 1992.

Meng, Z., P. Yang, G. W. Kattawar, L. Bi, K. N. Liou, and I. Laszlo (2010), Single−scattering properties of tri−axial ellipsoidal mineral dust aerosols: A database for application to radiative transfer calculations, J. Aerosol Sci., 41(5), 501–512, doi:10.1016/j.jaerosci.2010.02.008.10.1080/02786826.2019.1623863, 2020.

Mikuška, P., Večeřa, Z., Bartošíková, A., and Maenhaut, W.: Annular diffusion denuder for simultaneous removal of gaseous organic compounds and air oxidants during sampling of carbonaceous aerosols, Analytica Chimica Acta, 714, 68−75, https://doi.org/10.1016/j.aca.2011.11.054, 2012.

Moore, R. H., Wiggins, E. B., Ahern, A. T., Zimmerman, S., Montgomery, L., Campuzano Jost, P., Robinson, C. E., Ziemba, L. D., Winstead, E. L., Anderson, B. E., Brock, C. A., Brown, M. D., Chen, G., Crosbie, E. C., Guo, H., Jimenez, J. L., Jordan, C. E., Lyu, M., Nault, B. A., Rothfuss, N. E., Sanchez, K. J., Schueneman, M., Shingler, T. J., Shook, M. A., Thornhill, K. L., Wagner, N. L., and Wang, J.: Sizing response of the Ultra−High Sensitivity Aerosol Spectrometer (UHSAS) and Laser Aerosol Spectrometer (LAS) to changes in submicron aerosol composition and refractive index, Atmos. Meas. Tech., 14, 4517–4542, https://doi.org/10.5194/amt−14−4517−2021, 2021.

Osborne, S. R., Johnson, B. T., Haywood, J. M., Baran, A. J., Harrison, M. a. J. and 13McConnell, C. L.: Physical and optical properties of mineral dust aerosol during the 14Dust and Biomass−burning Experiment, J. Geophys. Res., 15113(D23), doi:10.1029/2007JD009551, 2008

Perim de Faria, J., Bundke, U., Berg, M., Freedman, A., Onasch, T. B., and Petzold, A.: Airborne and laboratory studies of an IAGOS instrumentation package containing a modified CAPS particle extinction monitor, Aerosol Science and Technology, 51, 1240−1253, 10.1080/02786826.2017.1355547, 2017.

Petzold, A., Rasp, K., Weinzierl, B., Esselborn, M., Hamburger, T., Dörnbrack, A., Kandler, K., Schütz, L., Knippertz, P., Fiebig, M. and Virkkula, A.: Saharan dust absorption and refractive index from aircraft−based observations during SAMUM 2006, 26Tellus B, 61(1), 118–130, doi:10.1111/j.1600−0889.2008.00383.x, 2009.

Petzold, A., P. Formenti, D. Baumgardner, U. Bundke, H. Coe, J. Curtius, P. J. DeMott, R. C. Flagan, M. Fiebig, J. G. Hudson, J. McQuaid, A. Minikin, G. C. Roberts, and J. Wang, In Situ Measurements of Aerosol Particles, In: Manfred Wendisch and Jean−Louis Brenguier (eds); Airborne Measurements for Environmental Research: Methods and Instruments, First Edition, Wiley−VCH Verlag GmbH & Co, 2013.

Pinnick, R. G., J. D. Pendleton and G. Videen, Response Characteristics of the Particle Measuring Systems Active Scattering Aerosol Spectrometer Probes, Aerosol Science & Technology, 33:4, 334−352, DOI: 10.1080/02786820050121530, 2000.

Radney, J. G., and Zangmeister, C. D.: Comparing Aerosol Refractive Indices Retrieved from Full Distribution and Size− and Mass−Selected Measurements, J. Q. Spec. Rad. Trans., 220, 10.1016/j.jqsrt.2018.1008.1021, 10.1016/j.jqsrt.2018.08.021, 2018.

Reid, J. S., Kinney Reid, J. S. and Hobbs, P. V.: Physical and optical properties of young smoke from individual biomass fires in Brazil, J. Geophys. Res., 103, 32 013–32 030, 1998.

Reid, J. S., Westphal, D. L., Holben, B. N., Welton, E. J., Tsay, S.−C., Eleuterio, D. P., Campbell, J. R., Christopher, S. A., Colarco, P. R., Jonsson, H. H., Livingston, J. M., Maring, H. B., Meier, M. L., Pilewskie, P., Prospero, J. M., Reid, E. A., Remer, L. A., Russell, P. B., Savoie, D. L., Smirnov, A., and Tanré, D.: Analysis of measurements of Saharan dust by airborne and ground−based remote sensing methods during the Puerto Rico Dust Experiment (PRIDE), J. Geophys. Res., 108, 8586, doi:10.1029/2002JD002493, 2003.

Reddington, C. L., Carslaw, K. S., Stier, P., Schutgens, N., Coe, H., Liu, D., Allan, J., Browse, J., Pringle, K. J., Lee, L. A., Yoshioka, M., Johnson, J. S., Regayre, L. A., Spracklen, D. V., Mann, G. W., Clarke, A., Hermann, M., Henning, S., Wex, H., Kristensen, T. B., Leaitch, W. R., Pöschl, U., Rose, D., Andreae, M. O., Schmale, J., Kondo, Y., Oshima, N., Schwarz, J. P., Nenes, A., Anderson, B., Roberts, G. C., Snider, J. R., Leck, C., Quinn, P. K., Chi, X., Ding, A., Jimenez, J. L., & Zhang, Q. (2017). The Global Aerosol Synthesis and Science Project (GASSP): Measurements and Modeling to Reduce Uncertainty, Bull. Amer. Meteor. Soc., 98(9), 1857−1877.

Rosenberg, P. D., A. R. Dean, P. I. Williams, J. R. Dorsey, A. Minikin, M. A. Pickering, and A. Petzold (2012), Particle sizing calibration with refractive index correction for light scattering optical particle counters and impacts upon PCASP and CDP data collected during the Fennec campaign, Atmos. Meas. Tech., 5(5), 1147–1163, doi:10.5194/amt−5−1147−2012.

Ryder, C. L., Highwood, E. J., Rosenberg, P. D., Trembath, J., Brooke, J. K., Bart, M., Dean, A., Crosier, J., Dorsey, J., Brindley, H., Banks, J., Marsham, J. H., McQuaid, J. B., Sodemann, H., and Washington, R.: Optical properties of Saharan dust aerosol and contribution from the coarse mode as measured during the Fennec 2011 aircraft campaign, Atmos. Chem. Phys., 13, 303−325, doi:10.5194/acp−13−303−2013, 2013.

Schafer, J. S., Eck, T. F., Holben, B. N., Thornhill, K. L., Ziemba, L. D., Sawamura, P., Moore, R. H., Slutsker, I., Anderson, B. E., Sinyuk, A., Giles, D. M., Smirnov, A., Beyersdorf, A. J., and Winstead, E. L.: Intercomparison of aerosol volume size distributions derived from AERONET ground−based remote sensing and LARGE in situ aircraft profiles during the 2011–2014 DRAGON and DISCOVER−AQ experiments, Atmos. Meas. Tech., 12, 5289–5301, https://doi.org/10.5194/amt−12−5289−2019, 2019.

© Author(s) 2021. CC BY 4.0 License.

Seinfeld, J. H., and Pandis, S. N.: Atmospheric chemistry and physics: From air pollution to climate change, in, John Wiley and Sons, Inc., New York, 1326, 2nd edition, 2006.

Shettle, E. P., and Fenn, R. W.: Models for the aerosols of the lower atmosphere and the effects of humidity variations on their optical properties., Air Force Geophysics Laboratory, U.S. Air Force Geophysics Laboratory, Hanscomb Air Force Base, Mass., Environmental Research Papers 670 AFGL−TR−79−0214, 1979.

Shiraiwa, Manabu, Kayo Ueda, Andrea Pozzer, Gerhard Lammel, Christopher J. Kampf, Akihiro Fushimi, Shinichi Enami, Andrea M. Arangio, Janine Fröhlich−Nowoisky, Yuji Fujitani, Akiko Furuyama, Pascale S. J. Lakey, Jos Lelieveld, Kurt Lucas, Yu Morino, Ulrich Pöschl, Satoshi Takahama, Akinori Takami, Haijie Tong, Bettina Weber, Ayako Yoshino, and Kei Sato, Aerosol Health Effects from Molecular to Global Scales, Environmental Science & Technology 51 (23), 13545−13567, DOI: 10.1021/acs.est.7b04417, 2017

Szymanski, W. W., and Liu, B. Y. H.: On the Sizing Accuracy of Laser Optical Particle Counters, Particle & Particle Systems Characterization, 3, 1−7, https://doi.org/10.1002/ppsc.19860030102, 1986.

Walser, A., Sauer, D., Spanu, A., Gasteiger, J. and Weinzierl, B.: On the parametrization of optical particle counter response including instrument−induced broadening of size spectra and a self−consistent evaluation of calibration measurements, Atmospheric Measurement Techniques, 10(11), 4341–4361, doi:https://doi.org/10.5194/amt−10−4341−142017, 2017.

Weinzierl, B., Ansmann, A., Prospero, J., Althausen, D., Benker, N., Chouza, F., Dollner, M., Farrell, D., Fomba, W., Freudenthaler, V., Gasteiger, J., Gross, S., Haarig, M., Heinold, B., Kandler, K., Kristensen, T., Mayol−Bracero, O. L., Müller, T., Reitebuch, O., Sauer, D., Schäfler, A., Schepanski, K., Spanu, A., Tegen, I., Toledano, C., and Walser, A.: The Saharan Aerosol Long−Range Transport and AerosoŒ Cloud−Interaction Experiment: Overview and Selected Highlights, Bulletin of the American Meteorological Society, 98, 1427−1451, 2017.

Wendisch, M., and J.−L. Brenguier, Airborne Measurements for Environmental Research, Wiley−VCH., 2013.

Wu, H., Taylor, J. W., Szpek, K., Langridge, J. M., Williams, P. I., Flynn, M., Allan, J. D., Abel, S. J., Pitt, J., Cotterell, M. I., Fox, C., Davies, N. W., Haywood, J., and Coe, H.: Vertical variability of the properties of highly aged biomass burning aerosol transported over the southeast Atlantic during CLARIFY−2017, Atmos. Chem. Phys., 20, 12697–12719, https://doi.org/10.5194/acp−20−12697−2020, 2020.

Zieger, P., Väisänen, O., Corbin, J. C., Partridge, D. G., Bastelberger, S., Mousavi−Fard, M., Rosati, B., Gysel, M., Krieger, U. K., Leck, C., Nenes, A., Riipinen, I., Virtanen, A. and Salter, M. E.: Revising the hygroscopicity of inorganic sea salt particles, Nature Communications, 8, 15883, doi:10.1038/ncomms15883, 2017.

https://doi.org/10.5194/amt-2021-403
Preprint. Discussion started: 15 December 2021
© Author(s) 2021. CC BY 4.0 License.
Atmospheric Measurement Techniques Discussions

Table 1. Technical characteristics of the OPCs considered in this paper.

Instrument	Size measurement range D_{EO} (µm)	Wavelength (nm)	Angular Range of scattered light	Calibration	Primary reference
PCASP−100	0.1−3.0 (31 channels)	632.8	35°–120°(direct beam) + 60°–145° (reflected beam)	PSL (1.59−0*i*)	Liu et al. (1992)
UHSAS	0.04 – 1 (99 channels)	1054	33° −75.2° + 104.8°−148°	PSL (1.59−0*i*)	Cai et al. (2008)
FSSP−300	0.275−20.5 (30 channels)	632.8	3°−15°	PSL (1.59−0*i*)	Baumgardner et al. (1992)
CDP-300	2−50 (30 channels)	658	4°−12°	Glass beads (1.59−0*i*)	Lance et al. (2010)
GRIMM model 1.109	0.25 – 32 (31 channels)	655[$]	30°−150° (direct beam) + 81°−98° (reflected beam)	PSL (1.59−0*i*)	Heim et al. (2008)
Sky−GRIMM model 1.129[#]	0.25 – 32 (31 channels)	655	30°−150° (direct beam) + 81°−98° (reflected beam)	PSL (1.59−0*i*)	Grimm and Eatough (2009)

[$] Company specifications. Heim et al. (2008) reported that the working wavelength of the GRIMM 1.109 is 683 nm.

[#] The technical characteristics of the GRIMM and Sky−OPC instruments relevant to this paper are identical and the calculations performed hold for both.

https://doi.org/10.5194/amt-2021-403
Preprint. Discussion started: 15 December 2021
© Author(s) 2021. CC BY 4.0 License.

Table 2. Calculated optical scattering, absorption and extinction coefficients (σ_{sca}, σ_{abs}, σ_{ext} expressed in Mm^{-1}; 1 Mm^{-1} = 10^{-6} m^{-1}), single scattering albedo (SSA, unitless) , mass extinction and absorption coefficients (MEC and MAC, respectively; units m^2 g^{-1}) obtained from Mie calculations for homogeneous spherical particles (*CRI* = 1.53 −0.003*i*) assuming the size distribution of mineral dust measured by the CDP (base case, see Fig.5) and two methods for correcting instances when the corrected values of dlog*D* become negative. Calculations are performed at wavelengths relevant to modelling and remote sensing products (440, 550 and 870 nm, and 10 μm).

	Base case				**Method 1 Grouping/widening**				**Method 2 Smoothing or fitting**			
	440	**550**	**870**	**10**	**440**	**550**	**870**	**10**	**440**	**550**	**870**	**10**
Scattering coeff. σ_{sca}	41.0	34.3	43.4	3.6	41.2	34.4	43.6	3.9	36.1	39.4	36.9	6.5
Absorption coeff. σ_{abs}	4.7	3.6	3.4	0.1	4.8	3.7	3.4	0.1	5.1	4.7	3.1	0.2
Extinction coeff. σ_{ext}	45.8	37.9	46.8	3.7	46.0	38.1	47.0	4.0	41.1	44.1	40.0	6.7
SSA	0.90	0.91	0.93	0.96	0.90	0.90	0.93	0.97	0.88	0.90	0.92	0.97
MEC	0.50	0.41	0.51	0.04	0.50	0.41	0.51	0.04	0.40	0.43	0.39	0.07
MAC	0.052	0.039	0.037	0.002	0.051	0.039	0.037	0.002	0.049	0.045	0.029	0.002

https://doi.org/10.5194/amt-2021-403
Preprint. Discussion started: 15 December 2021
© Author(s) 2021. CC BY 4.0 License.
Atmospheric Measurement Techniques Discussions

Table 3. Same as Table 2 for the Angstrom exponents for extinction and scattering (AEE and AEA, respectively; unitless) calculated between 440 and 870 nm, and mass concentration (M_c, expressed in μg m^{-3}).

	Base case	Method 1 Grouping/widening	Method 2 Smoothing or fitting
Angstrom exponent, extinction (AEE)	−0.031	−0.031	0.043
Angstrom exponent, absorption (AEA)	0.497	0.498	0.749
Mass concentration (M_c)	91.4	93.0	103.2

https://doi.org/10.5194/amt-2021-403
Preprint. Discussion started: 15 December 2021
© Author(s) 2021. CC BY 4.0 License.

Figure 1. Scattering cross section values, C_{sca}, as a function of particle diameter calculated using Mie theory for the CDP OPC considered in this paper. The black lines represent C_{sca} for the calibration particles (PSL and equivalent light−scattering material). The purple lines represent the C_{sca} function for absorbing urban aerosols (*CRI* = 1.56 – 0.087*i*), while the brown lines represent C_{sca} for moderately−absorbing mineral dust (*CRI* = 1.53 – 0.003*i*), and the light blue lines represent C_{sca} for marine aerosols (*CRI* = 1.38 – 0.001*i*). The dotted line represents a single C_{sca} value which corresponds many values of particle diameter, represented by the coloured arrows.

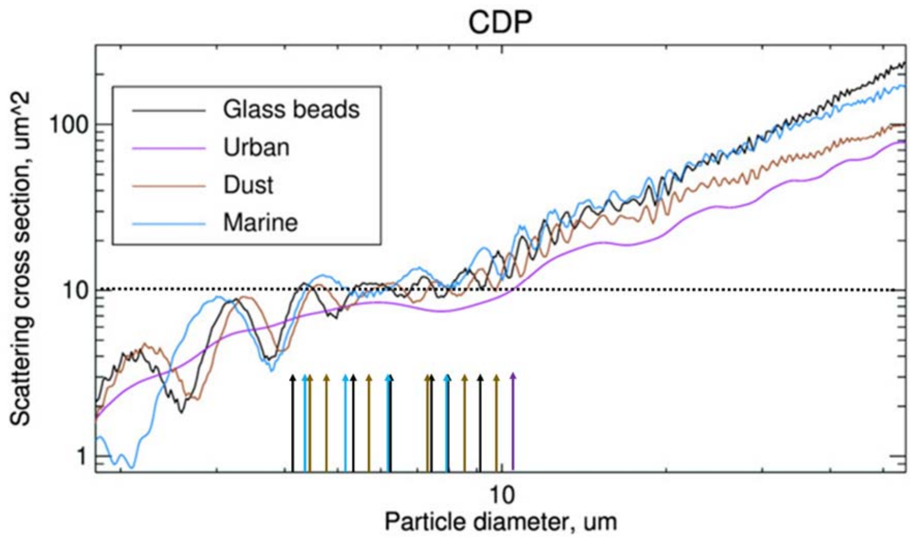

https://doi.org/10.5194/amt-2021-403
Preprint. Discussion started: 15 December 2021
© Author(s) 2021. CC BY 4.0 License.

Atmospheric Measurement Techniques
Discussions

Figure 2. (Top in each group) Scattering cross sections, C_{sca}, as a function of particle diameter for the OPCs considered in this paper. The black lines represent C_{sca} for the calibration particles (PSL and equivalent light−scattering material). The purple lines represent the C_{sca} function for absorbing urban aerosols (*CRI* = 1.56 – 0.087*i*), while the brown lines represent C_{sca} for moderately−absorbing mineral dust (*CRI* = 1.53 – 0.003*i*), and the light blue lines represent C_{sca} or marine aerosols (*CRI* = 1.38 – 0.001*i*). The symbols represent the average C_{sca} over the nominal size bins of each OPC, whose boundaries are illustrated by the vertical thick grey lines.

(Bottom in each group) Absolute values of the first derivative in log−space of C_{sca} versus the bin width dlog*D*, which is a measure of the sensitivity of the instrument to particle size.

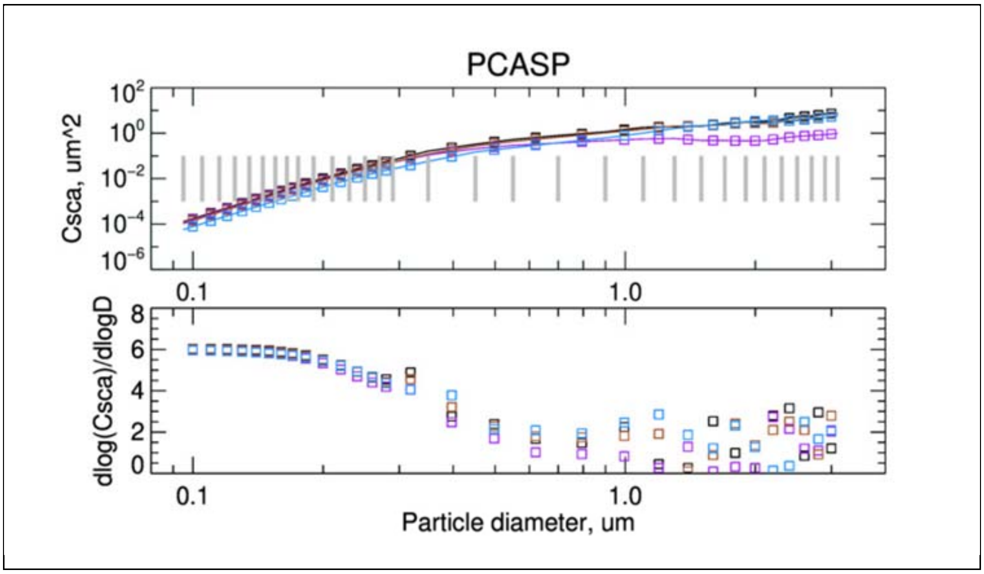

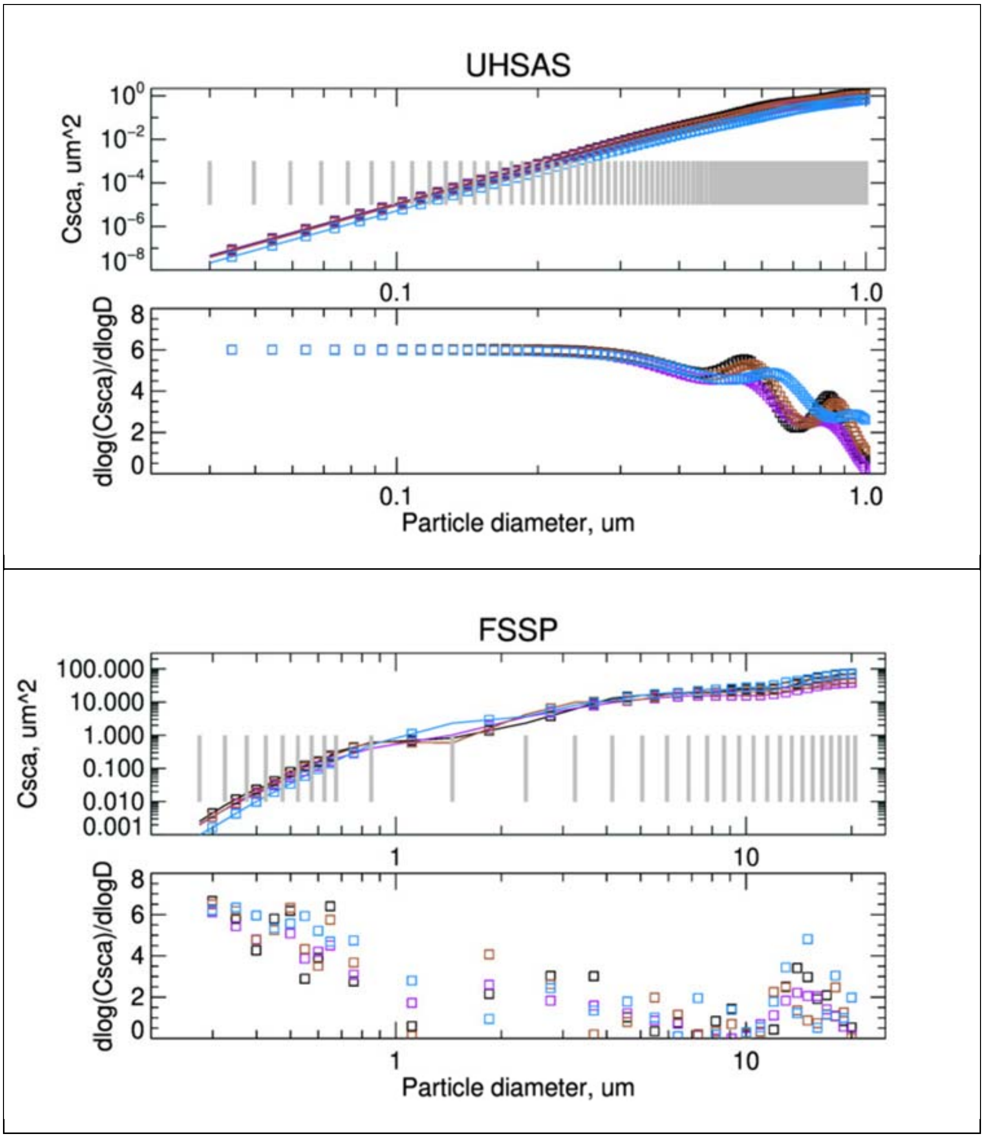
UHSAS
Csca, um^2
dlog(Csca)/dlogD
0.1
1.0
Particle diameter, um
FSSP
100.000
10.000
1.000
0.100
0.010
0.001
1
10

https://doi.org/10.5194/amt-2021-403
Preprint. Discussion started: 15 December 2021
© Author(s) 2021. CC BY 4.0 License.

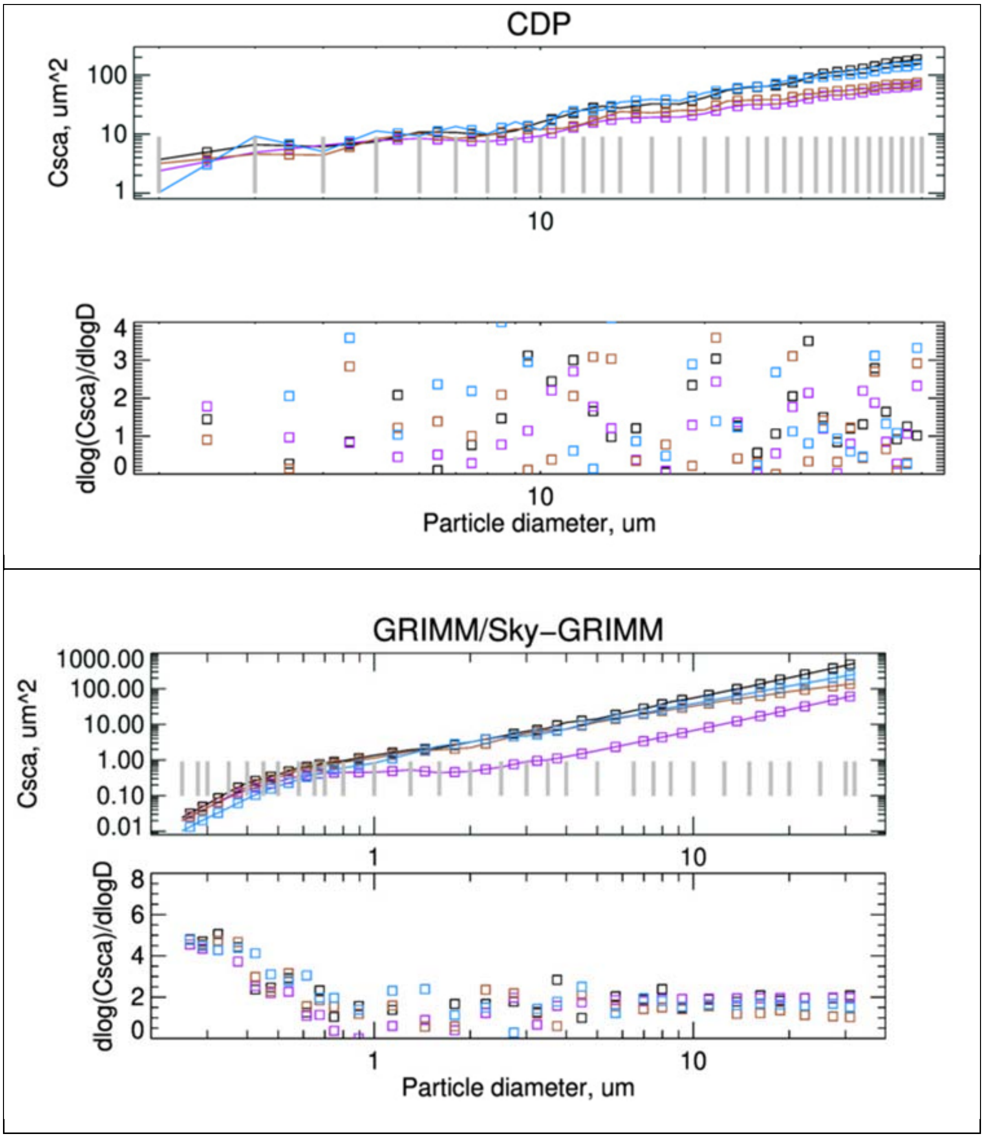

746

https://doi.org/10.5194/amt-2021-403
Preprint. Discussion started: 15 December 2021
© Author(s) 2021. CC BY 4.0 License.

Figure 3. Scattering cross sections, C_{sca}, as a function of particle diameter for the OPCs considered in this paper for moderately−absorbing mineral dust (*CRI* = 1.53 – 0.003*i*). The brown line represents C_{sca} calculated by Mie theory assuming homogeneous spherical particles, while the orange line represents C_{sca} calculated according to Huang et al. (2021) assuming homogeneous aspherical ellipsoid particles.

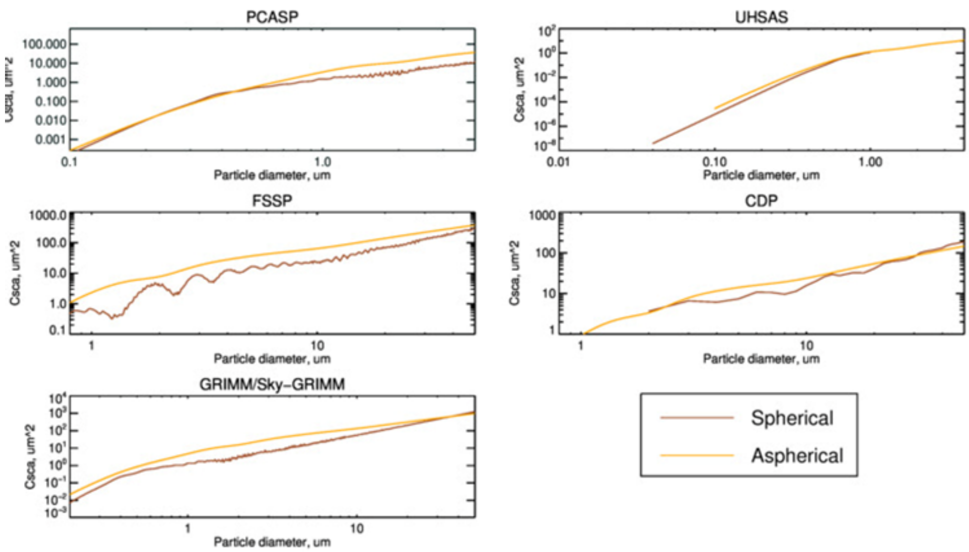

https://doi.org/10.5194/amt-2021-403
Preprint. Discussion started: 15 December 2021
© Author(s) 2021. CC BY 4.0 License.
Atmospheric Measurement Techniques
Discussions

Figure 4. Scatterplot of geometric−equivalent bin size boundary (D_{geo}) corresponding to the *CRI* of the example aerosol types (mineral dust, urban and marine) compared to the optical−equivalent bin size boundary (D_{EO}) obtained if the calibration *CRI* is used. For mineral dust, values are shown for both the aspherical and spherical approximation (brown and yellow lines, respectively).

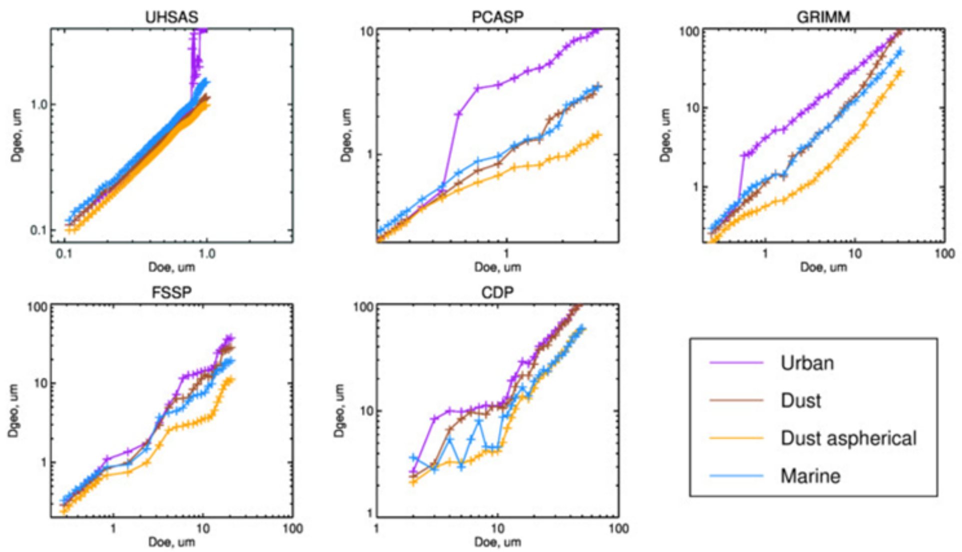

https://doi.org/10.5194/amt-2021-403
Preprint. Discussion started: 15 December 2021
© Author(s) 2021. CC BY 4.0 License.

Atmospheric Measurement Techniques
Discussions

Figure 5. Representation of a model log−normal size distribution of mineral dust (see Seinfeld and Pandis, 2006) for the CDP, taking into account the corrected bin diameter. The first panel (left) shows the relationship between the corrected and the calibration bin diameters for a *CRI* of 1.53−0.*003i*. The middle panel shows the behaviour of the corrected dlog*D* with calibration bin diameter, while the right panel shows the representation of the size distribution using the corrected CDP evaluation of particle size. The red box indicates the discontinuity of the size distribution around a diameter of 10 µm.

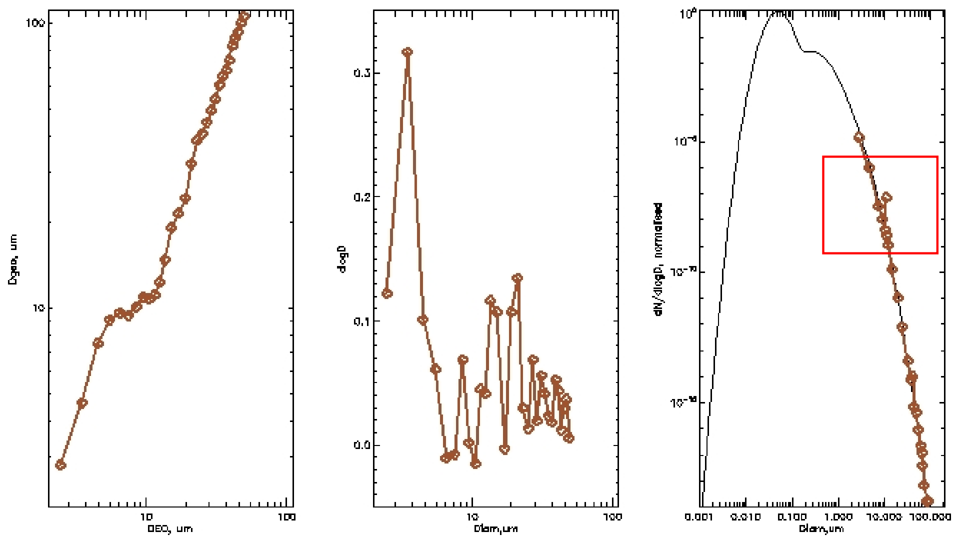

https://doi.org/10.5194/amt-2021-403
Preprint. Discussion started: 15 December 2021
© Author(s) 2021. CC BY 4.0 License.

Figure 6. Correction methods in the CDP measurements for the caes of *CRI* of mineral dust (1.53 – 0.003*i*). The base case is based on simply discarding the values of d*N*/dlog*D* corresponding to negative values of dlog*D*. The left panels (from top to bottom) correspond to the application of Method 1, that is, grouping instances where *dlogD* was negative to create a wider bin to which the sum of the particle counts of the original bins was attributed. The right panels correspond to the application of Method 2, that is, fitting of the D_{bin} curves with a second−degree polynomial function adapted to three size ranges (below 2.43 μm, in between 2.43 and 16.85 μm and above 16.85 μm, see Annex 1 for fit parameters). Panels show, from top to bottom: (1) the size range of application for all the CDP channels; (2) the resulting dlog*D*; (3) the resulting d*N*/dlog*D* for the full size range and (4) for a restricted size range.